

Article

Validation of a SPICE Model for High Frequency Electroporation Systems

Paulius Butkus *, Sonata Tolvaišienė and Sebastjanas Kurčevskis

Department of Electrical Engineering, Faculty of Electronics, Vilnius Gediminas Technical University, Sauletekio al. 11, Vilnius 10221, Lithuania; sonata.tolvaisiene@vgtu.lt (S.T.); sebastjanas.kurcevskis@vgtu.lt (S.K.)

* Correspondence: paulius.butkus@vgtu.lt; Tel.: +370-680-51-641

Received: 29 May 2019; Accepted: 20 June 2019; Published: 23 June 2019



Abstract: In this paper, we present an analysis and a validation of a simulation program with integrated circuit emphasis (SPICE) model for a pulse forming circuit of a high frequency electroporation system, which can deliver square-wave sub-microsecond (100–900 ns) electric field pulses. The developed SPICE model is suggested for use in evaluation of transient processes that occur due to high frequency operations in prototype systems. A controlled crowbar circuit was implemented to support a variety of biological loads and to ensure a constant electric pulse rise and fall time during electroporation to be independent of the applied buffer bioimpedance. The SPICE model was validated via a comparison of the simulation and experimental results obtained from the already existing prototype system. The SPICE model results were in good agreement with the experimental results, and the model complexity was found to be sufficient for analysis of transient processes. As result, the proposed SPICE model can be useful for evaluation and compensation of transient processes in sub-microsecond pulsed power set-ups during the development of new prototypes.

Keywords: electroporation; SPICE model; pulsed electric field; high-voltage generator

1. Introduction

High-pulsed electric fields (PEFs), used to induce an electric field across a cell membrane, have many applications [1–6]. However, PEF application in electroporation has mostly been researched in the field of medicine and the food industry [7,8]. The electroporation phenomenon, induced by a PEF, is driven by the reorientation of lipids and formation of pores in the cell membrane, resulting in an increase in cell permeability [9]. Thus, higher cell absorption of drugs and genes can be achieved as a result of increased molecular transportation via the cell membrane [10]. For this reason, the use of electroporation is gaining momentum, and new medical applications are emerging at an increasing rate.

In order to trigger the intended electroporation processes, the typical transmembrane voltage threshold is 200 mV or higher [11,12]. This is acquired through accumulation of sufficient charge during electric pulsing, which allows for the membrane permittivity to change. After the threshold is reached, the electroporation phenomenon is initiated. As a result, electroporation is a pulse-dependent phenomenon [13,14], which can be investigated using electric circuit models. A biological cell can be represented as an electrical resistor–capacitor (RC) circuit, wherein the RC value represents the cell and the suspension charging constant.

The electroporation process is only initiated effectively after the induced steady state transmembrane voltage is reached. Hence, the desired effect and efficiency of the electroporation process for medical applications depends on specific pulse parameters, such as the electric pulse duration (varies from tens of ns to ms range), pulse number, repetition frequency, direction of the generated pulse (monopolar, bipolar), electric field amplitude (varies from millivolt up to several kilovolt range) and shape of the pulse [14–20].

Usually, a trade-off between the PEF amplitude and duration is made under a certain pulse repetition number, but the proper PEF application protocol is influenced by the cell type in general [21,22]. For instance, for mammalian cells, a well-established protocol is to apply a burst of microsecond pulses (e.g. $100\ \mu\text{s} \times 8$) in the kV/cm PEF strength range [22,23]. However, in recent years, numerous researchers have started to focus on shorter (sub-microsecond) but higher intensity (range of kV) PEF pulses [24–26]. The reasoning for this is based on the ability to use generated pulse energy more efficiently—due to reduced thermal influence—as well as to have the possibility of bypassing the plasma membrane to affect a cell's inner organelles directly [27–29]. Additional interest into the use of high-voltage sub-microsecond PEFs lies in the possibility of inducing cell apoptosis [30,31]. However, one of the most particular focuses is in biomedical applications (e.g., improvement of electrochemotherapy and tissue ablation protocols) [22].

Different PEF waveforms have been applied in electroporation techniques, such as square-wave (rectangular), exponential decay, triangular and sinusoidal waveforms. However, it has been demonstrated that square-wave and exponential decay pulses have higher efficiency in comparison with other types of pulses [32]. As a result, a majority of PEF generators produce pulses in one of these two types of waveforms. However, further studies have reported that square-wave pulses are more efficient during the application of high intensity (tens to hundreds of kV/cm) nanosecond PEFs, due to its enhanced control of the pulse energy [33]. This is an important aspect for the rapidly growing microfluidics-based electroporation technique [34], wherein planar electrode structures have proved to be advantageous [34,35].

Most pulsed electric field generators available in the market for commercial use are made for specific PEF application, with predefined pulsed parameters and limited control possibility. These specifications limit the possibilities for application in the electroporation research area, where higher flexibility for setting different protocols is required. The development of a flexible, high-frequency electroporation system, aligned with advanced planar electrodes, could contribute toward further investigation of biomedical techniques with medical applications.

Therefore, in this study, we analyzed a simulation program with integrated circuit emphasis (SPICE) model of a pulse forming circuit of a high frequency electroporation system, which was capable of delivering square-wave sub-microsecond (100–900 ns) electric field pulses. A SPICE model, which was introduced in previous study [36], was further developed and a validation test was performed via a comparison of simulation and experimental results obtained from the prototype system. The SPICE model results were in good agreement with the experimental results. In addition, the complexity of the developed SPICE model was sufficient for analysis of transient processes. Our simulation model contributes to the prototyping of flexible electroporation systems, and can be applied for evaluation and compensation of transient processes in the emerging sub-microsecond pulsed power set-ups by reducing the time and costs associated with the prototyping phase.

2. PEF Generator Specifications

As mentioned, the PEF parameter requirements for an electroporation system depend on the intended biological processes, which are meant to be induced by high electric fields in biological objects. The pulse parameters, such as the electric field strength, pulse amplitude, duration, waveform and repetition frequency, are selected according to the requirements of the experiments. Therefore, in this study, considering the development in electroporation research specified above, we were aiming to develop and present an electroporator system capable of generating single and burst PEF pulses of variable duration in the range of 100 ns to 1 ms. This range of controllable PEF pulse duration would ensure that the device was flexible and therefore applicable in a wide area of electroporation research activities.

As mentioned, use of a short pulse duration means a trade-off with PEF amplitude must be made. A short pulse duration (in range of 100 ns) increases the required electric field strength needed to reach the transmembrane voltage threshold due to the amount of energy involved. Consequently, the

application of sub-microsecond pulses requires an electric field strength of at least 30 kV/cm. In the case wherein standard 1 mm electroporation cuvettes are used, a high-voltage power supply (in the range of at least 2–3 kV) has to be applied to reach a sufficient electric field strength. However, as the overall aim of a variable and controllable PEF typically remains, the pulse forming circuit should be able to deliver adjustable power PEF pulses with a voltage level ranging from 0 kV to 3 kV.

Additionally, it is expected that a biological load will vary from 50 Ω to 500 Ω during experimental applications. Meanwhile, the peak value of a pulsed electric current should not exceed 60 A at the lowest expected load and at the maximum voltage range. This requirement is determined by the current handling capability and induced Joule heating on biological object, which negatively impact the electroporation process [37]. Therefore, high-energy pulses are rarely used.

Furthermore, since the efficiency of some treatment applications can be dependent on the pulse frequency, the device should be capable of altering the pulse frequency over an extensive range. Thus, we decided that the PEF frequency range had to be adjustable from 1 Hz to 3.5 MHz. Moreover, in order to have good control of the pulse energy, the square-wave pulse form was preferred, and repeated pulses had to have identical form. Based on all the requirements specified above, a summary of the pulse forming circuit requirements is provided in Table 1.

Table 1. Pulse forming circuit requirements.

Parameter	Value
Pulse amplitude	1 V to 3 kV
Electric field strength	≤ 30 kV/cm
Number of pulses	1–99
Repetition frequency	1 Hz to 3.5 MHz
Pulse duration	100 ns to 1 ms
Current	0–60 A

3. SPICE Model of the PEF Generator

3.1. Design of the Pulse Forming Circuit

Designing a flexible pulse forming circuit for an electroporation system is a challenging and multidisciplinary task. It requires application of numerical methods to investigate the electrical circuit's transient processes and parasitic elements, such as the contact capacitance, resistance of the transmission line and stray inductance. Inappropriate application of compensation circuits may lead to the appearance of overvoltage, overcurrent or waveform distortion, as well as over-damped or under-damped responses. These would result in a poorly performing pulse forming circuit. Hence, to compensate for the transient processes that occur during turn-on and turn-off time, which appear due to parasitic circuit parameters, proper compensation circuits must be developed [38]. Moreover, load matching and driving circuit topologies for the semiconductor switches should be solved.

In order to investigate and design the measures needed to compensate the parasitic circuit parameter's influence on the PEF generator, the commercially free LTSpice simulation software was used to create a SPICE model of the pulse forming circuit. The developed SPICE model of the pulse forming circuit for the PEF generator is presented in Figure 1. Considering the high frequency requirements described in previous section, the pulse forming circuit switching control was limited to the high-frequency semiconductor MOSFET switches, which are suitable to ensure high dV/dt .

Synchronized control of the MOSFET switches was ensured via the usage of a microprocessor, which also provided the user with the ability to precisely define the electric field strength, duration range, pulse number and frequency. Thus, the PEF generator was able output either a single short square-wave pulse or a number of multiple pulses. As seen in Figure 1, the pulse forming circuit consisted of three main groups:

- A pulse driving circuit unit, which was composed of an ADUM4223 isolated gate driver (Analog Devices, Norwood, USA). This gate driver is designed for higher switching speeds and provides reliable control over the switching characteristics of MOSFET switches.
- A pulse power circuit, which was composed of six high speed and low capacitance C2M0080120D silicon carbide power MOSFET switches (SW1–SW6, CREE, Durham, USA), manufactured by CREE. This type of switch ensures high system switching frequency.
- A high-voltage DC power supply supported by the capacitor array, for energy accumulation.

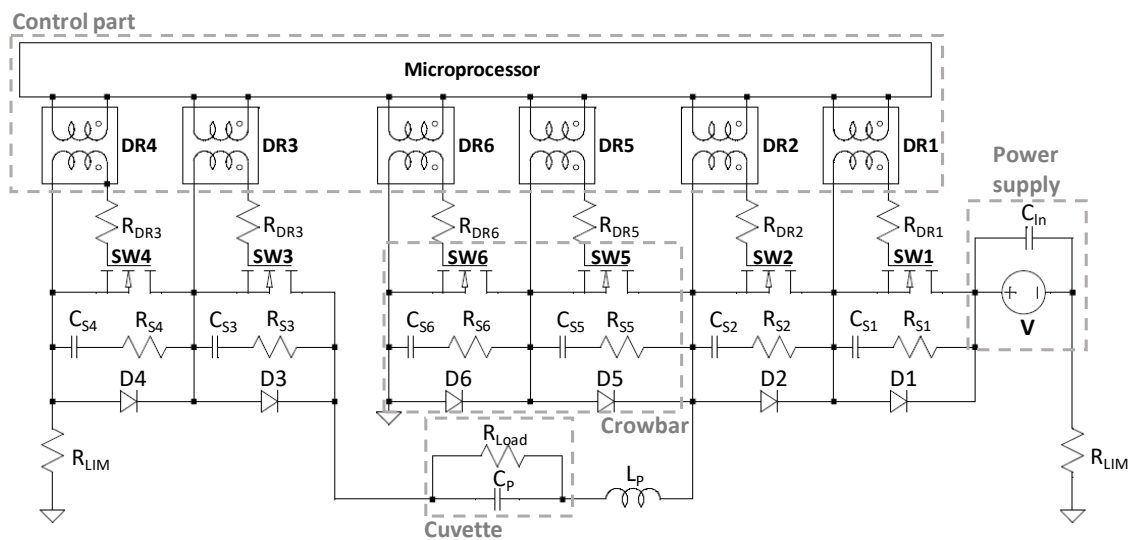


Figure 1. The simplified simulation program with integrated circuit emphasis (SPICE) pulse forming circuit for the pulsed electric field (PEF) generator.

The SW1–SW6 switches were employed to form the square-wave pulses. For the compensation circuit, snubber diodes D1 to D6 were implemented in parallel to each MOSFET switch to provide reverse voltage protection. In addition, energy absorbing RC snubber circuits were connected in parallel to each MOSFET switch in order to eliminate sudden voltage surges in the pulse forming circuit created by stray inductance and to ensure MOSFET synchronization. This type of compensation circuit ensures proper surge voltage damping during turn-on and turn-off time, thereby protecting the power MOSFET switches and other devices in its vicinity.

The semiconductor switches were driven by commercially available two-channel MOSFET drivers DR1–DR6, ensuring the galvanical isolation of the control circuit. In the SPICE model, to imitate the galvanic isolation, the MOSFET switches were connected to the pulse control unit throughout the power transformers (transformation ratio equal to 1) and current limiting resistors, R_{DR} . The pulse driving circuit unit (control part shown in Figure 1) represents the up-to-4 A output, current-isolated, half-bridge gate ADUM4223 driver, providing control over the MOSFET switches with a frequency up to 3.5 MHz, output drive voltage ranging from 4.5 V to 18 V, and an isolation capability up to 5 kV. As a result, the driving circuit ensured precise and reliable control of the switching characteristics.

The crowbar circuit, which operated in synchronous mode with SW3 and SW4, was introduced to ensure short pulse fall time and independence from the load (a more detail operational performance is explained in the following section). To ensure a good match of switching characteristics between the SPICE model and the PEF generator prototype system, the SPICE model of C2M0080120D silicon carbide power MOSFET switch from CREE (USA) was used during the simulations, because the same type of switch was used in the prototype system. This switch was also used for SPICE model validation. Each C2M0080120D switch was capable of handling voltages up to 1.7 kV and currents up to 72 A. Furthermore, all of the MOSFET switches were paired in series to be able to withstand commutation voltages up to 3 kV.

The parasitic snubber circuit capacitance (C_S) and the parasitic circuit inductance (L_P) of the printed circuit board (PCB) circuit were, respectively, represented by a capacitor and an inductor connected to the pulse forming circuit in series. In addition, the load resistance (R_{LOAD}) and parasitic load capacitance (C_P) imitated the cell and the suspension charging constant. In order to simulate real electroporation experiment parameters, where low conductivity buffers are used, the load of the SPICE model was varied from 50 Ω to 500 Ω . The main parameters of the created SPICE model of the PEF generator are shown in Table 2.

Table 2. Pulse forming circuit requirements.

Parameter	Min. Value	Max. Value	Final Value
Snubber resistance (R_S)	0.1 Ω	20 Ω	0.5 Ω
Snubber capacitance (C_S)	200 pF	900 pF	500 pF
Load (R_{LOAD})	50 Ω	500 Ω	50–500 Ω
Parasitic load capacitance (C_P)	10 pF	100 pF	50 pF
Parasitic circuit inductance (L_P)	1 μ H	5 μ H	1.2 μ H

In order to suppress the transient processes of the pulse forming circuit, the parameters shown in Table 2 were swept from the minimum to the maximum values. The impact of each parameter was evaluated to not only find the optimal RC snubber circuit parameters, but also to have a good match with the measurement values obtained from the actual PEF generator prototype system.

3.2. The Pulse Forming Circuit Operational Description

Switches SW1–SW2 and SW3–SW4 belonged to the main power line (see Figure 1) and were responsible for commutation of the power source voltage over the load. When these MOSFET switches were turned on, a high-voltage pulse was over the load. Consequently, all of these switches operated in a synchronized mode and, thus, were opened and closed at the same time. The pulse rise time was dependent on the switching characteristics of the switches, as well as the parasitic circuit inductance and capacitance.

The switches SW5–SW6 represented a controllable crowbar circuit, which was triggered by DR5–DR6 at the same time as when the pulse power circuit switches in the pairs SW1–SW2 and SW3–SW4 were closed. In this way, the crowbar circuit could be opened to create a new path for the high current to flow to the ground, avoiding a path through the cuvette—since this path was closed at the same time by SW1–SW2 and SW3–SW4. As a result, the pulse fall time became independent of the load, but was influenced by the switching characteristics of the switches and the parasitic parameters of the circuit.

The resulting pulse on the load of 100 Ω with the implemented crowbar circuit is shown in Figure 2. The SPICE model simulation results indicated that the crowbar circuit reduced the pulse fall time from 30 ns to 18 ns; the controllable and synchronized crowbar circuit minimized the fall time of the pulse. It removed the characteristic load-dependent tail and provided an opportunity for sub-microsecond pulse generation with a high impedance buffer.

In this way, the presented pulse forming circuit offered flexibility for different experimental applications, while the SPICE model itself was suitable for the electrical pulse forming circuit transient processes and analysis of the parasitic elements.

As will be demonstrated below, the SPICE model was also able to optimize prototype development and reduce the time and cost needs during the prototype development phase.

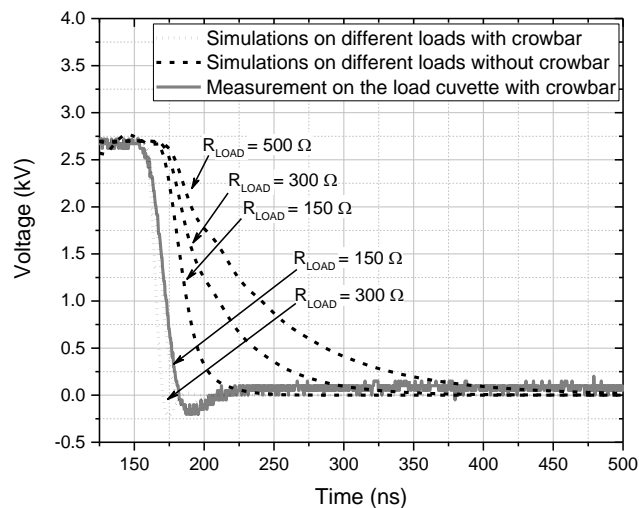


Figure 2. The comparison of pulse fall time with and without the crowbar circuit under different loads.

3.3. The Impact of the RC Snubber Circuit

Parasitic line inductance and parasitic load capacitance have a negative impact on the performance of pulse forming circuits and can impose transient processes of overvoltage and overcurrent. In addition, other undesirable pulse distortions, like circuit ringing, can be triggered. As a result, the generation of 3 kV square electric pulses for PEF electroporation treatment applications is complicated and a multidisciplinary engineering task, which cannot be solved without a proper set-up of RC snubber circuits. Figure 3 presents the parasitic circuit inductance influence on the pulse, which resulted in overvoltage during turn-on and turn-off of the semiconductor MOSFET switches.

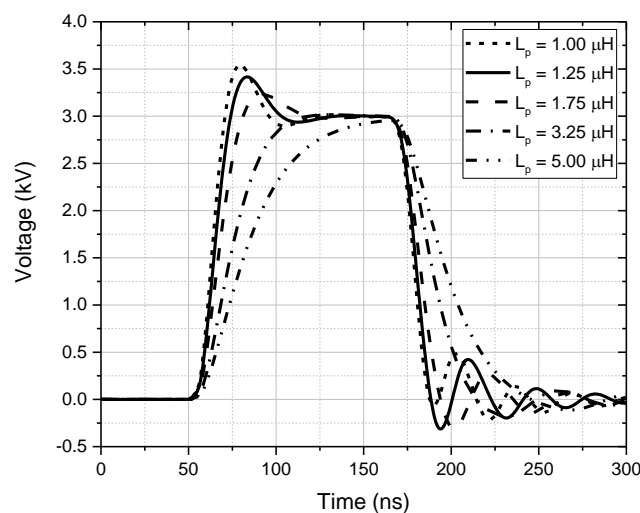


Figure 3. The output voltage pulse on the load of 150 Ω without the snubber and crowbar circuits.

One of the main tasks during the development of the sub-microsecond square-wave PEF generator was to compensate the transient processes in the pulse forming circuit during the rise and fall time of the generated pulse. To solve this issue, RC snubber circuits were implemented into the pulse forming circuit and connected in parallel with the semiconductor MOSFET switches. In addition, the RC snubber circuits provided synchronization of the series-connected switches. In the prototype development phase, the design of optimal RC snubber circuits can be a time consuming and costly task if the different set-ups of RC snubber circuits are experimentally tested directly on the prototype system. On the other hand, this task can be more easily solved via application of a proper simulation

model (such as a SPICE model). However, the developed SPICE model has to be validated to be trusted for use in the design phase of any new prototype system.

4. SPICE Model Validation

The prototype of a flexible PEF generator addressing all of the requirements discussed above has already been developed for the study of electroporation in previous research [26,39]. In this study, the same PEF generator was used to verify the SPICE model presented above by performing a comparison of the numerical and experimental results of the output pulse.

As a first step of validation, a single compensated output pulse on the load of $100\ \Omega$ was simulated with the SPICE model under different RC snubber circuit parameters and compared with the measured single output pulse of the PEF generator prototype system. The PEF generator output signal on the $100\ \Omega$ load cuvette was measured using the 1:100 probe and a DPO4034 digital oscilloscope (Tektronix, Beaverton, OR, USA). To capture the output waveform, the experimental results were recorded as a mean of five measurements.

The results of the comparison are presented in Figure 4, which shows the measured output pulse of the developed PEF generator prototype system and two simulation curves with swept snubber resistance, R_s . The single 2.5 kV output pulse waveform at the minimum duration of the existing PEF generator was used for this comparison. As seen in Figure 4, the pulse duration (measured at 50% of the pulse amplitude) was 90 ns ($\pm 10\%$). It was limited by the MOSFET switches switching characteristics and the parasitic parameters of the circuit. A rise time of 28 ns and a fall time of 18 ns was measured (10–90% of the pulse amplitude). The measured values matched well with the simulation results, underlining the influence of the crowbar circuit on output voltage.

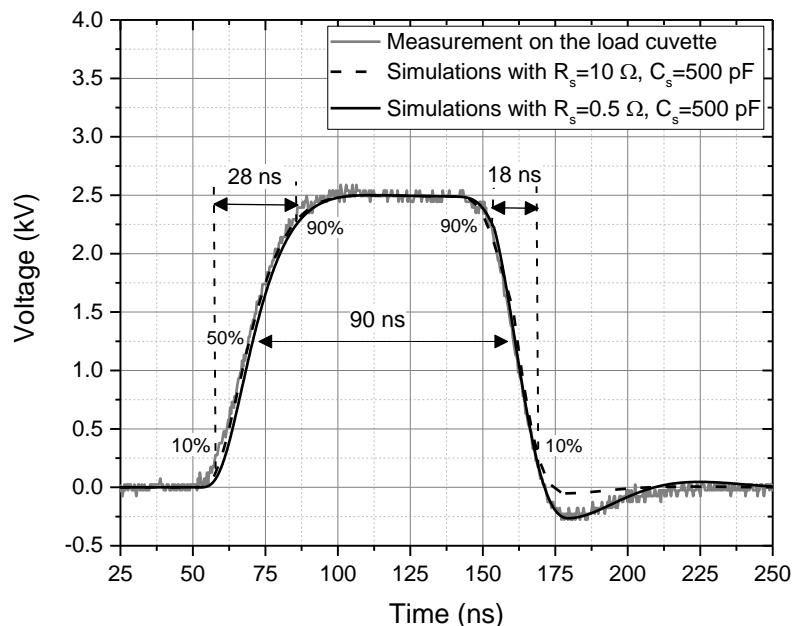


Figure 4. The comparison of simulation and experimental results of a single electrical pulse waveform generated by the PEF generator.

In addition, as seen in Figure 4, the snubber resistance of $10\ \Omega$ and the snubber capacitance of 500 pF resulted in a faster turn-off time and better minimization of the reverse overvoltage; however, the snubber resistance of $0.5\ \Omega$ with 500 pF snubber capacitance fit better with the measured signal. These results suggest that the RC snubber circuits used in the prototype system were not optimally designed. In any case, the implemented RC circuit helped to suppress a transient process and limit the reverse overvoltage during the fall time of the pulse, while the new SPICE model was proved to be sufficient for the prototyping of new PEF generators.

As an additional step for SPICE model validation, a comparison of the simulated and generated series of PEF pulses was performed at the highest frequency (3.5 Hz) and voltage (3 kV) output. The PEF generator output signal on the 100 Ω load cuvette was also measured using the 1:100 probe and the DPO4034 digital oscilloscope (Tektronix, Beaverton, OR, USA). To capture the output waveform, the experimental results were recorded as a mean of five measurements. The SPICE model simulations were performed under the same load and supply voltage conditions as the measured experimental data in order to be able to compare the numerical results with the measured values. The results of this validation step are presented in Figure 5.

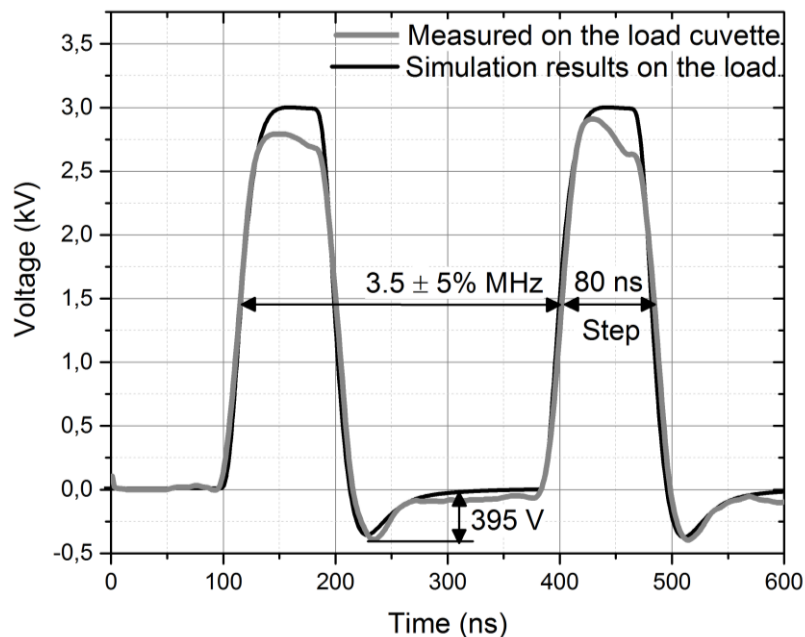


Figure 5. Simulation and experimental results of the PEF generator's high-voltage sub-microsecond output pulses on the load of 100 Ω with repetition frequency up to 3.5 MHz.

In Figure 5 we can see the measured 3 kV output pulse of the developed PEF generator. It appears that pulses with a duration of 80 ns (measured on 50% of the pulse amplitude) and a rise and fall time of 25 ns and 18 ns, respectively, were generated. The developed prototype system of the PEF generator was capable of generating pulses with a frequency up to 3.5 MHz. In Figure 5, it can be seen that the simulation results of the SPICE model were in good agreement with the measured output signal of the prototype system. Thus, our model may be considered sufficient for analyzing transient processes in electroporation systems and can be used in the prototype design phase of new PEF generators.

5. Conclusions

In this paper, we presented an analysis and a validation of a SPICE model for a pulse forming circuit of a high frequency electroporation system, which was controlled by high-frequency MOSFET switches and was capable of delivering square-wave sub-microsecond PEF pulses. The SPICE model was developed to be used for the evaluation of pulse forming circuit transient processes, which occur as a consequence of high frequency operation, and for the optimization of RC snubber circuit design in future PEF generators. A controlled crowbar circuit was implemented to support a variety of biological loads and to ensure a constant rise and fall time during electroporation, independent of the applied buffer bioimpedance. The SPICE model was validated via a comparison of simulation and experimental results obtained from the prototype system. The SPICE model results were in good agreement with the experimental results and the model complexity was proved to be sufficient for analysis of transient processes. The results of this study and the validated SPICE model will contribute to the evaluation and compensation of the transient processes in sub-microsecond pulsed power set-ups, as well as

the development of new prototypes. Future work should continue with development and validation of the planar electrodes simulation model, which would allow for simulation of a wider range of experimental conditions in electroporation research.

Author Contributions: Conceptualization, P.B. and S.T.; methodology, P.B.; software, P.B.; validation, P.B., S.T. and S.K.; formal analysis, P.B.; investigation, P.B.; data curation, P.B.; writing—original draft preparation, P.B.; writing—review and editing, P.B., S.T. and S.K.; visualization, P.B.; supervision, S.T.

Funding: This research received no external funding.

Conflicts of Interest: The authors declare no conflict of interest.

References

1. Akiyama, H.; Sakugawa, T.; Namihira, T.; Takaki, K.; Minamitani, Y.; Shimomura, N. Industrial applications of pulsed power technology. *IEEE Trans. Dielectr. Electr. Insul.* **2007**, *14*, 1051–1064. [[CrossRef](#)]
2. Jang, S.-R.; Ryoo, H.-J.; Ok, S.-B. Pulsed-power system for leachate treatment applications. *J. Power Electron.* **2011**, *11*, 612–619. [[CrossRef](#)]
3. Barba, F.J.; Parniakov, O.; Pereira, S.A.; Wiktor, A.; Grimi, N.; Boussetta, N.; Saraiva, J.A.; Raso, J.; Martin-Belloso, O.; Witrowa-Rajchert, D.; et al. Current applications and new opportunities for the use of pulsed electric fields in food science and industry. *Food Res. Int.* **2015**, *77*, 773–798. [[CrossRef](#)]
4. Schoenbach, K.H.; Katsuki, S.; Stark, R.H.; Buescher, E.S.; Beebe, S.J. Bioelectrics-new applications for pulsed power technology. *IEEE Trans. Plasma Sci.* **2002**, *30*, 293–300. [[CrossRef](#)]
5. Gómez, B.; Munekata, P.E.S.; Gavahian, M.; Barba, F.J.; Martí-Quijal, F.J.; Bolumar, T.; Campagnol, P.C.B.; Tomasevic, I.; Lorenzo, J.M. Application of pulsed electric fields in meat and fish processing industries: An overview. *Food Res. Int.* **2019**, *123*, 95–105. [[CrossRef](#)]
6. Sitzmann, W.; Vorobiev, E.; Lebovka, N. Applications of electricity and specifically pulsed electric fields in food processing: historical backgrounds. *Innov. Food Sci. Emerg. Technol.* **2016**, *37*, 302–311. [[CrossRef](#)]
7. Yarmush, M.L.; Golberg, A.; Serša, G.; Kotnik, T.; Miklavčič, D. Electroporation-Based technologies for medicine: Principles, applications, and challenges. *Annu. Rev. Biomed. Eng.* **2014**, *16*, 295–320. [[CrossRef](#)] [[PubMed](#)]
8. Hart, F.X.; Palisano, J.R. The application of electric fields in biology and medicine. In *Electric Field*; InTech Open: London, UK, 2018.
9. Tsong, T.Y. Electroporation of cell membranes. *Biophys. J.* **1991**, *60*, 297–306. [[CrossRef](#)]
10. Haberl, S.; Miklavcic, D.; Sersa, G.; Frey, W.; Rubinsky, B. Cell membrane electroporation—part 2: The applications. *IEEE Electr. Insul. Mag.* **2013**, *29*, 29–37. [[CrossRef](#)]
11. Teissié, J.; Rols, M.P. An experimental evaluation of the critical potential difference inducing cell membrane electroporation. *Biophys. J.* **1993**, *65*, 409–413. [[CrossRef](#)]
12. Murovec, T.; Sweeney, D.C.; Latouche, E.; Davalos, R.V.; Brosseau, C. Modeling of Transmembrane potential in realistic multicellular structures before electroporation. *Biophys. J.* **2016**, *111*, 2286–2295. [[CrossRef](#)] [[PubMed](#)]
13. Kotnik, T.; Pucihar, G.; Rebersek, M.; Miklavcic, D.; Mir, L.M. Role of pulse shape in cell membrane electroporation. *Biochim. Biophys. Acta* **2003**, *1614*, 193–200. [[CrossRef](#)]
14. Pucihar, G.; Krmelj, J.; Reberšek, M.; Napotnik, T.B.; Miklavčič, D.; Reberšek, M.; Napotnik, T.B.; Miklavčič, D. Equivalent pulse parameters for electroporation. *IEEE Trans. Biomed. Eng.* **2011**, *58*, 3279–3288. [[CrossRef](#)] [[PubMed](#)]
15. Rebersek, M.; Faurie, C.; Kanduser, M.; Corović, S.; Teissié, J.; Rols, M.-P.; Miklavcic, D. Electroporation with automatic change of electric field direction improves gene electrotransfer in-vitro. *Biomed. Eng. Online* **2007**, *6*, 25. [[CrossRef](#)] [[PubMed](#)]
16. Kotnik, T.; Kramar, P.; Pucihar, G.; Miklavcic, D.; Tarek, M. Cell membrane electroporation—part 1: The phenomenon. *IEEE Electr. Insul. Mag.* **2012**, *28*, 14–23. [[CrossRef](#)]
17. Krassowska, W.; Filev, P.D. Modeling electroporation in a single cell. *Biophys. J.* **2007**, *92*, 404–417. [[CrossRef](#)]
18. Kotnik, T.; Pucihar, G.; Miklavčič, D. Induced Transmembrane voltage and its correlation with electroporation-mediated molecular transport. *J. Membr. Biol.* **2010**, *236*, 3–13. [[CrossRef](#)]

19. Towhidi, L.; Kotnik, T.; Pucihar, G.; Firoozabadi, S.M.P.; Mozdarani, H.; Miklavčič, D. Variability of the minimal transmembrane voltage resulting in detectable membrane electroporation. *Electromagn. Biol. Med.* **2008**, *27*, 372–385. [[CrossRef](#)]
20. Schoenbach, K.H.; Pakhomov, A.G.; Semenov, I.; Xiao, S.; Pakhomova, O.N.; Ibey, B.L. Ion Transport into cells exposed to monopolar and bipolar nanosecond pulses. *Bioelectrochemistry* **2015**, *103*, 44–51. [[CrossRef](#)]
21. Dean, D.A. Cell-specific targeting strategies for electroporation-mediated gene delivery in cells and animals. *J. Membr. Biol.* **2013**, *246*, 737–744. [[CrossRef](#)]
22. Novickij, V.; Ruzgys, P.; Grainys, A.; Šatkauskas, S. High frequency electroporation efficiency is under control of membrane capacitive charging and voltage potential relaxation. *Bioelectrochemistry* **2018**, *119*, 92–97. [[CrossRef](#)] [[PubMed](#)]
23. Ruzgys, P.; Novickij, V.; Novickij, J.; Šatkauskas, S. Nanosecond range electric pulse application as a non-viral gene delivery method: Proof of concept. *Sci. Rep.* **2018**, *8*, 15502. [[CrossRef](#)] [[PubMed](#)]
24. Garner, A.L.; Caiafa, A.; Jiang, Y.; Klopman, S.; Morton, C.; Torres, A.S.; Loveless, A.M.; Naculaes, V.B. Design, characterization and experimental validation of a compact, flexible pulsed power architecture for ex vivo platelet activation. *PLoS ONE* **2017**, *12*, e0181214. [[CrossRef](#)] [[PubMed](#)]
25. Tan, Y.; Yang, H.; Wu, J.; Yang, X.; Zhang, Y.; Zeng, G.; Zhang, X. The sub-microsecond pulser applied for electroporation effect. *Sheng Wu Yi Xue Gong Cheng Xue Za Zhi* **2012**, *29*, 615–619. [[PubMed](#)]
26. Novickij, V.; Zinkevičienė, A.; Perminaitė, E.; Čėsna, R.; Lastauskienė, E.; Paškevičius, A.; Švedienė, J.; Markovskaja, S.; Novickij, J.; Girkontaitė, I. Non-invasive nanosecond electroporation for biocontrol of surface infections: An in vivo study. *Sci. Rep.* **2018**, *8*, 14516. [[CrossRef](#)] [[PubMed](#)]
27. Deng, J.; Schoenbach, K.H.; Buescher, E.S.; Hair, P.S.; Fox, P.M.; Beebe, S.J. The effects of intense submicrosecond electrical pulses on cells. *Biophys. J.* **2003**, *84*, 2709–2714. [[CrossRef](#)]
28. Schoenbach, K.; Hargrave, B.; Joshi, R.; Kolb, J.; Nuccitelli, R.; Osgood, C.; Pakhomov, A.; Stacey, M.; Swanson, R.; White, J.; et al. Bioelectric effects of intense nanosecond pulses. *IEEE Trans. Dielectr. Electr. Insul.* **2007**, *14*, 1088–1109. [[CrossRef](#)]
29. Beebe, S.J.; Chen, Y.-J.; Sain, N.M.; Schoenbach, K.H.; Xiao, S. Transient features in nanosecond pulsed electric fields differentially modulate mitochondria and viability. *PLoS ONE* **2012**, *7*, e51349. [[CrossRef](#)] [[PubMed](#)]
30. Pakhomova, O.N.; Gregory, B.W.; Semenov, I.; Pakhomov, A.G. Two modes of cell death caused by exposure to nanosecond pulsed electric field. *PLoS ONE* **2013**, *8*, e70278. [[CrossRef](#)]
31. Beebe, J.S. Mechanisms of nanosecond pulsed electric field (NsPEF)-induced cell death in cells and tumors. *J. Nanomed. Res.* **2015**, *2*, 00016. [[CrossRef](#)]
32. Miklavcic, D.; Towhidi, L. Numerical study of the electroporation pulse shape effect on molecular uptake of biological cells. *Radiol. Oncol.* **2010**, *44*, 34–41. [[CrossRef](#)] [[PubMed](#)]
33. Kandušer, M.; Miklavčič, D. *Electroporation in Biological Cell and Tissue: An Overview*; Springer: Berlin, Germany, 2009; pp. 1–37.
34. Geng, T.; Lu, C. Microfluidic electroporation for cellular analysis and delivery. *Lab Chip* **2013**, *13*, 3803–3821. [[CrossRef](#)] [[PubMed](#)]
35. Novickij, V.; Tabošnikov, A.; Smith, S.; Grainys, A.; Novickij, J.; Tolvaišienė, S.; Markovskaja, S. Feasibility of parylene coating for planar electroporation copper electrodes. *Mater. Sci.* **2017**, *23*, 93–97. [[CrossRef](#)]
36. Butkus, P.; Kurcevskis, S.; Tolvaišienė, S.; Grainys, A. Computer model of the high frequency up to 30 KV/Cm electric field generator. In Proceedings of the 2017 5th IEEE Workshop on Advances in Information, Electronic and Electrical Engineering (AIEEE), Riga, Latvia, 24–25 November 2017; pp. 1–3.
37. Pliquett, U.; Nuccitelli, R. Measurement and simulation of joule heating during treatment of B-16 Melanoma tumors in mice with nanosecond pulsed electric fields. *Bioelectrochemistry* **2014**, *100*, 62–68. [[CrossRef](#)] [[PubMed](#)]
38. Novickij, V.N.; Stankevic, V.; Grainys, A.; Novickij, J.; Tolvaišienė, S. Microsecond electroporator optimization for parasitic load handling and damping. *Elektron. Elektrotechnol.* **2015**, *21*, 40–43.
39. Novickij, V.; Grainys, A.; Butkus, P.; Tolvaišienė, S.; Švedienė, J.; Paškevičius, A.; Novickij, J. High-frequency submicrosecond electroporator. *Biotechnol. Biotechnol. Equip.* **2016**, *30*, 607–613. [[CrossRef](#)]

